

Dear Author,

Here are the proofs of your article.

- You can submit your corrections **online**, via **e-mail** or by **fax**.
- For **online** submission please insert your corrections in the online correction form. Always indicate the line number to which the correction refers.
- You can also insert your corrections in the proof PDF and **email** the annotated PDF.
- For fax submission, please ensure that your corrections are clearly legible. Use a fine black pen and write the correction in the margin, not too close to the edge of the page.
- Remember to note the **journal title**, **article number**, and **your name** when sending your response via e-mail or fax.
- **Check** the metadata sheet to make sure that the header information, especially author names and the corresponding affiliations are correctly shown.
- **Check** the questions that may have arisen during copy editing and insert your answers/ corrections.
- **Check** that the text is complete and that all figures, tables and their legends are included. Also check the accuracy of special characters, equations, and electronic supplementary material if applicable. If necessary refer to the *Edited manuscript*.
- The publication of inaccurate data such as dosages and units can have serious consequences. Please take particular care that all such details are correct.
- Please **do not** make changes that involve only matters of style. We have generally introduced forms that follow the journal's style. Substantial changes in content, e.g., new results, corrected values, title and authorship are not allowed without the approval of the responsible editor. In such a case, please contact the Editorial Office and return his/her consent together with the proof.
- If we do not receive your corrections **within 48 hours**, we will send you a reminder.
- Your article will be published **Online First** approximately one week after receipt of your corrected proofs. This is the **official first publication** citable with the DOI. **Further changes are, therefore, not possible.**
- The **printed version** will follow in a forthcoming issue.

#### **Please note**

After online publication, subscribers (personal/institutional) to this journal will have access to the complete article via the DOI using the URL: [http://dx.doi.org/\[DOI\]](http://dx.doi.org/[DOI]).

If you would like to know when your article has been published online, take advantage of our free alert service. For registration and further information go to: <http://www.link.springer.com>.

Due to the electronic nature of the procedure, the manuscript and the original figures will only be returned to you on special request. When you return your corrections, please inform us if you would like to have these documents returned.

# Metadata of the article that will be visualized in OnlineFirst

ArticleTitle	Prenucleation at the Interface Between MgO and Liquid Magnesium: An <i>Ab Initio</i> Molecular Dynamics Study	
Article Sub-Title		
Article CopyRight	The Author(s) (This will be the copyright line in the final PDF)	
Journal Name	Metallurgical and Materials Transactions A	
Corresponding Author	Family Name	<b>Fan</b>
	Particle	
	Given Name	<b>Z.</b>
	Suffix	
	Division	BCAST
	Organization	Brunel University London
	Address	Uxbridge, Middlesex, UB8 3PH, UK
	Phone	+44 1895 266406
	Fax	
	Email	Zhongyun.Fan@brunel.ac.uk
	URL	
	ORCID	
Author	Family Name	<b>Fang</b>
	Particle	
	Given Name	<b>C. M.</b>
	Suffix	
	Division	BCAST
	Organization	Brunel University London
	Address	Uxbridge, Middlesex, UB8 3PH, UK
	Phone	
	Fax	
	Email	
	URL	
	ORCID	
Schedule	Received	3 December 2018
	Revised	
	Accepted	
Abstract	<p>Magnesia (MgO) particles inevitably exist in liquid Mg and may be used as potential sites for heterogeneous nucleation to achieve effective grain refinement. Understanding of the atomic configurations on MgO surfaces and in the liquid Mg adjacent to the liquid Mg/MgO interfaces is therefore of both scientific and practical interests. We investigate the surface structures of MgO in liquid Mg and the atomic arrangements of liquid Mg adjacent to liquid/substrate interfaces, using an <i>ab initio</i> molecular dynamics (MD) simulation technique. We find that an atomically rough terminating Mg layer forms on the {1 1 1} terminated MgO substrate (octahedral MgO) in liquid Mg. The simulations also reveal that on the structurally flat {0 0 1} terminated MgO substrate (cubic MgO) a rough Mg layer forms due to the unique chemical interactions between the ions on the substrate and the liquid metals. The surface roughness</p>	

together with the large lattice misfits with solid Mg makes both octahedral and cubic MgO substrates impotent for heterogeneous nucleation of  $\alpha$ -Mg. The present results may shed new light on grain refinement of Mg-alloys.

---

Footnote Information

Manuscript submitted 3 December, 2018.

---

# 2 3 Prenucleation at the Interface Between MgO 4 and Liquid Magnesium: An *Ab Initio* Molecular 5 Dynamics Study



6  
7 C.M. FANG and Z. FAN

8  
9 Magnesia (MgO) particles inevitably exist in liquid Mg and may be used as potential sites for  
10 heterogeneous nucleation to achieve effective grain refinement. Understanding of the atomic  
11 configurations on MgO surfaces and in the liquid Mg adjacent to the liquid Mg/MgO interfaces  
12 is therefore of both scientific and practical interests. We investigate the surface structures of  
13 MgO in liquid Mg and the atomic arrangements of liquid Mg adjacent to liquid/substrate  
14 interfaces, using an *ab initio* molecular dynamics (MD) simulation technique. We find that an  
15 atomically rough terminating Mg layer forms on the {1 1 1} terminated MgO substrate  
16 (octahedral MgO) in liquid Mg. The simulations also reveal that on the structurally flat {0 0 1}  
17 terminated MgO substrate (cubic MgO) a rough Mg layer forms due to the unique chemical  
18 interactions between the ions on the substrate and the liquid metals. The surface roughness  
19 together with the large lattice misfits with solid Mg makes both octahedral and cubic MgO  
20 substrates impotent for heterogeneous nucleation of  $\alpha$ -Mg. The present results may shed new  
21 light on grain refinement of Mg-alloys.

22  
23 <https://doi.org/10.1007/s11661-019-05495-4>  
24 © The Author(s) 2019

## 26 I. INTRODUCTION

27 **G**RAIN refinement is usually desirable during metal  
28 casting since it not only facilitates the casting processes,  
29 but also accomplishes a grain refined microstructure  
30 with reduced cast defects, which in turn enhances  
31 mechanical performance of as-cast components.<sup>[1-4]</sup> A  
32 well-established approach to grain refinement enhances  
33 heterogeneous nucleation by addition of grain refiners  
34 which contain potent solid particles as nucleation  
35 sites.<sup>[1,2]</sup> A typical example is the grain refinement of  
36 Al-free Mg-alloys by addition of Mg-Zr master  
37 alloys.<sup>[2,4-10]</sup> Zr is iso-structural to Mg with a small  
38 lattice misfit (0.67 pct), and therefore Zr particles should  
39 act as potent nucleation sites for  $\alpha$ -Mg during solidifi-  
40 cation according to the epitaxial nucleation model.<sup>[11]</sup>  
41 Recently, a new concept of grain refinement was  
42 introduced based on the concept of explosive grain  
43 initiation, in which the most effective grain refinement  
44 can be achieved by the least potent particles if there exist  
45 no other more potent particles of significance in the  
46 melt.<sup>[12]</sup> This new approach to grain refinement can be  
47 best demonstrated by grain refinement of Mg-alloys by

the native MgO particles.<sup>[13]</sup> Without addition of any  
grain refiner, high pressure die casting of commercial  
purity Mg resulted in an average grain size of 6  $\mu\text{m}$ .<sup>[12]</sup>  
To understand better such experimental results and to  
obtain new insight into the heterogeneous nucleation  
process, it is essential to have detailed knowledge about  
the surface structures of MgO particles in contact with  
liquid Mg and the atomic arrangement in the liquid  
adjacent to the liquid Mg/MgO interfaces (denoted as  
L-Mg/MgO interfaces hereafter).

Magnesia (MgO) particles always exist in Mg melts  
due to the high affinity between O and Mg. MgO has a  
NaCl-type structure. It is a typical ionic crystal and  
belongs to the family of MX (M represents a metallic  
element, X an element of high electronegativity). The  
ionic MX crystals under ambient conditions have a  
stable {0 0 1} surface termination (denoted as MX{0 0  
1} hereafter), which contains equal numbers of  $\text{M}^{n+}$   
and  $\text{X}^{n-}$  ions and therefore are non-polar.<sup>[14]</sup> A cleavage  
along the MX [1 1 1] termination produces two smooth  
surfaces: one with the X surface termination, the other  
with X surface termination, with both surfaces being  
polar. Such polar surfaces are unstable under ambient  
conditions, but can be stabilized by defects, *e.g.*, M or X  
domains.<sup>[15]</sup> However, the situation may become differ-  
ent when an ionic crystal is in a liquid metal environ-  
ment. The free electrons of the liquid metal can  
eliminate the polar effect and stabilize the polar surfaces,  
such as in the case of MgO{1 1 1} in liquid Mg. MgO{1  
1 1} surfaces have a two dimensional hexagonal lattice,

C.M. FANG and Z. FAN are with the BCAST, Brunel University  
London, Uxbridge, Middlesex UB8 3PH, United Kingdom. Contact e-  
mail: Zhongyun.Fan@brunel.ac.uk

Manuscript submitted 3 December, 2018.

78 the same as that of the close packed Mg{0 0 1} plane.  
79 However, there exists a large lattice misfit between  
80 MgO{1 1 1} and Mg{0 0 1} (8.2 pct),<sup>[12,16]</sup> rendering  
81 MgO particles impotent for heterogeneous nucleation of  
82 Mg.

83 There have been both experimental and modeling  
84 efforts to understand the nucleation of  $\alpha$ -Mg on native  
85 MgO particles.<sup>[13,16-21]</sup> Native MgO particles in Mg  
86 melts have two distinctive morphologies: octahedron  
87 with {1 1 1} surface terminations (denoted as MgO{1 1  
88 1}) and cubic with the {0 0 1} surface terminations  
89 (denoted as MgO{0 0 1}).<sup>[12,13,16-19]</sup> Experimental inves-  
90 tigations by high-resolution transmission electron  
91 microscopy (HRTEM) have confirmed that there exist  
92 specific orientation relations (ORs) between the MgO  
93 substrates and the solid Mg. This suggests that fcc MgO  
94 can act as sites for heterogeneous nucleation of hcp  
95  $\alpha$ -Mg. First-principles approaches were used to explore  
96 mainly the wetting and adhesion for different crystal  
97 orientations between solid  $\alpha$ -Mg and MgO.<sup>[20-22]</sup> In  
98 order to understand the structural effect on prenucleation  
99 at atomic level, Men and Fan<sup>[23,24]</sup> performed  
100 atomistic molecular dynamics (MD) simulations on the  
101 atomic ordering in a liquid metal adjacent to a smooth  
102 substrate of different lattice misfits. Their simulations  
103 showed that the structural effect is strong on the  
104 in-plane atomic ordering but weak on the atomic  
105 layering in the liquid adjacent to the substrate. A  
106 smooth substrate surface of a smaller misfit provides  
107 better structural templating for heterogeneous nucleation,  
108 in agreement with the epitaxial nucleation  
109 model.<sup>[11]</sup> Recently we investigated the chemical effect  
110 of potent substrates on prenucleation and found that a  
111 chemically affinitive substrate promotes prenucleation in  
112 the liquid at the liquid/substrate interface, whereas a  
113 chemically repulsive substrate impedes it.<sup>[25]</sup> In addition,  
114 Jiang *et al.*<sup>[26]</sup> modeled the effect of substrate surface  
115 roughness on prenucleation using a classic atomistic  
116 MD technique. Their modeling revealed that atomic  
117 level surface roughness impedes significantly prenucleation.  
118<sup>[26]</sup> In light of such findings, it would be interesting  
119 to investigate the effect of interaction between MgO and  
120 liquid Mg on the prenucleation at the L-Mg/MgO  
121 interface.

122 In this paper, we investigate systematically the prenucleation  
123 phenomenon in L-Mg/MgO{1 1 1} and L-Mg/  
124 MgO{0 0 1} systems using a parameter-free *ab initio*  
125 molecular dynamics (AIMD) technique. The simulation  
126 results suggest that both MgO{1 1 1} and MgO{0 0 1}  
127 are impotent for heterogeneous nucleation of  $\alpha$ -Mg.  
128 Such information is not only helpful to understand  
129 heterogeneous nucleation theory in general, but also  
130 facilitates the development of effective approaches to  
131 grain refinement of Mg-alloys.

## 132 II. SIMULATION METHODS

### 133 A. Setting Up Supercells for Simulations

134 Periodic boundary conditions were employed in the  
135 structural optimizations and the AIMD simulations. A

hexagonal supercell was built based on the relation of  $a$  136  
 $\approx 3.615a_o$ , where  $a_o$  is the lattice parameter of the fcc 137  
MgO.<sup>[27]</sup> The substrate is composed of four O layers and 138  
three Mg layers (O-terminated) or four O layers and five 139  
Mg layers (Mg-terminated). In this way the hexagonal 140  
supercell has  $a = 14.90 \text{ \AA}$ , and  $c = 64.62 \text{ \AA}$ , and contains 141  
425 Mg and 100 O for the L-Mg/MgO{1 1 1} 142  
systems, with consideration of the thermal expansion of 143  
both MgO and Mg at 1000K.<sup>[27,28]</sup> The melting temper- 144  
ature of Mg is 650°C or 923K at ambient pressure. 145  
Similarly, a tetragonal supercell with  $a = 16.85 \text{ \AA}$  and 146  
 $c = 35.05 \text{ \AA}$  was built for the L-Mg/MgO{0 0 1} 147  
system. This supercell contains 320 atoms in liquid Mg 148  
and 192 atoms in MgO substrate. We employed these 149  
large supercells in order to avoid risk of artificial 150  
crystallization of the liquid Mg, and to achieve a good 151  
balance between the simulations reliability and the 152  
computational capability. 153

### 154 B. Quantifying Atomic Ordering in the Melt Adjacent 155 to a Substrate

To quantitatively describe the atomic ordering of the 156  
liquid Mg adjacent to the substrates, two different 157  
parameters were used.<sup>[23,29]</sup> One is the atomic density 158  
profile,  $\rho(z)$ : 159

$$\rho(z) = \langle N_z(t) \rangle / (L_x L_y \Delta z), \quad [1]$$

where  $L_x$  and  $L_y$  are the  $x$  and  $y$  dimensions of the cell, 161  
respectively, and  $z$  the dimension perpendicular to the 162  
interface,  $\Delta z$  the bin width, and  $N_z(t)$  the number of 163  
particles between  $z - (\Delta z/2)$  and  $z + (\Delta z/2)$  at time  $t$ . 164  
 $\langle N_z(t) \rangle$  indicates a time-averaged number of particles. 165  
The atomic density profile,  $\rho(z)$ , describes atomic 166  
ordering along the  $z$ -direction. 167

Another one is the in-plane order parameter,  $S(z)$ , 168  
which is used to quantify the degree of atomic ordering 169  
in each layer and is defined as<sup>[23,29]</sup>: 170

$$S(z) = [\sum \exp(i\mathbf{Q} \cdot \mathbf{r}_j)]^2 / N_z^2, \quad [2]$$

where the summation is over all atoms within a given 172  
bin of width  $\Delta z$ ,  $\mathbf{Q}$  is the reciprocal lattice vector, and  $\mathbf{r}_j$  173  
is the Cartesian coordinates of the  $j$ th atom in space,  $N_z$  174  
the number of atoms in the bin.  $S(z)$  quantifies the 175  
atomic ordering in a plane parallel to the interface. 176

### 177 C. Simulation Technique and Settings

In this study, we employed a pseudo-potential 178  
plane-wave approach within the first-principles den- 179  
sity-functional theory (DFT) code Vienna *ab initio* 180  
Simulation Package (VASP).<sup>[30,31]</sup> The VASP code uses 181  
the projector augmented-wave (PAW) method.<sup>[32,33]</sup> The 182  
exchange and correlation terms are described using the 183  
generalized gradient approximation (GGA-PBE).<sup>[34]</sup> 184  
The atomic electronic configurations in pseudo-poten- 185  
tials are Mg ([Ne] 3s<sup>2</sup>3p<sup>0</sup>) and O ([He] 2s<sup>2</sup>2p<sup>4</sup>). The 186  
cut-off energies for the wave functions and for the 187  
augmentation functions for structural optimizations 188  
were 400.0 and 600.0 eV, respectively. The electronic 189

190 wave functions were sampled on dense grids, *e.g.*, a  
 191  $24 \times 24 \times 24$   $k$ -mesh (365  $k$ -points) in the irreducible  
 192 Brillouin zone (BZ) of the conventional face-centered  
 193 cubic (fcc) cell of MgO using the Monkhorst–Pack  
 194 approach.<sup>[35]</sup> The present method allows variable frac-  
 195 tional occupation numbers. Therefore, it works well for  
 196 metallic systems. This code has been successfully applied  
 197 to simulate metallic/insulating transition,<sup>[30,31]</sup> as well as  
 198 solid/liquid interface systems.<sup>[25]</sup> The *ab initio* MD  
 199 simulation is based on the finite-temperature den-  
 200 sity-functional theory of the one-electron states. It is  
 201 also based on the exact energy minimization and  
 202 calculation of the exact Hellmann–Feynman forces after  
 203 each MD step using the preconditioned conjugate  
 204 techniques, and the Nosé dynamics for generating a  
 205 canonical NVT ensemble.<sup>[30]</sup> For the *A/MD* simulations  
 206 of the large supercells, we employed a cut-off energy of  
 207 320 eV for the L-Mg/MgO systems, and only the  
 208  $\Gamma$ -point in the BZs to balance the demand of compu-  
 209 tations for obtaining reliable results and capability of  
 210 the computer cluster. Test simulations using different  
 211 cut-off energies ranging from 200.0 to 400.0 eV have  
 212 shown that the present settings are reasonable.

213 The liquid Mg of the systems was generated by  
 214 equilibrating for 3000 steps (1.5 fs per step) at 3000K.  
 215 The equilibrated liquid Mg at high temperature was then  
 216 cooled to the designed temperatures. The obtained liquid  
 217 Mg and the substrates were used to build the simulation  
 218 systems for equilibrating at the designed temperature for  
 219 about 6000 to 8000 steps (about 10 ps). It is well known  
 220 that for complex liquid/solid systems, a meaningful  
 221 statistical analysis cannot be drawn from a single model,  
 222 and conclusions based on limited configuration-sampling  
 223 might be misleading.<sup>[25,30,36,37]</sup> In the present study, we  
 224 used several different starting structures, and employed  
 225 the time-averaged method to sample the system with over  
 226 a period of time up to 4.5 ps (3000 steps) to obtain  
 227 meaningful results. All substrate and liquid atoms were  
 228 fully relaxed during the simulations.

### 229 III. RESULTS

230 The first-principles DFT structural optimizations  
 231 were conducted to calculate lattice parameters of both  
 232 hcp  $\alpha$ -Mg and fcc MgO. The calculated lattice param-  
 233 eters for  $\alpha$ -Mg are  $a = 3.192$  Å and  $c = 5.185$  Å, which  
 234 are very close to the experimental values of  
 235  $a = 3.2094$  Å,  $c = 5.2108$  Å in the literature.<sup>[28]</sup> The  
 236 calculated lattice parameter for the MgO is  
 237  $a = 4.246$  Å, which is again very close to the experi-  
 238 mental value of  $a = 4.212$  Å.<sup>[27]</sup> Both calculations  
 239 reproduced the experimental values well within 1 pct  
 240 of error, confirming the validity of the current simula-  
 241 tion approaches.

#### 242 A. Surface Structures of the MgO Substrates in Liquid 243 Mg

244 The MgO{1 1 1} surface has two potential atomic  
 245 configurations; one is O-terminated (denoted as MgO{1  
 246 1 1}<sub>O</sub>) and the other one is Mg-terminated (denoted as

MgO{1 1 1}<sub>Mg</sub>). In this work we have simulated atomic  
 247 arrangements in liquid Mg adjacent to both MgO{1 1  
 248 1 1}<sub>O</sub> and MgO{1 1 1}<sub>Mg</sub> substrates. Figure 1 shows the  
 249 evolutions of atomic arrangements at the L-Mg/MgO{1  
 250 1 1} interfaces during the *A/MD* simulations at 1000K.  
 251

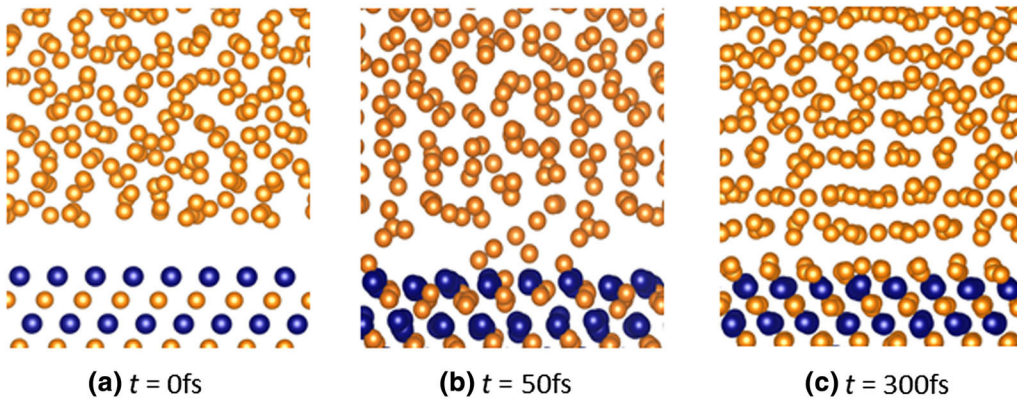
252 The Mg atoms in the liquid adjacent to the MgO{1 1  
 253 1 1}<sub>O</sub> substrate approach quickly the surface of MgO{1 1  
 254 1 1}<sub>O</sub> substrate (Figures 1(a) through (c)). A stable Mg  
 255 layer forms on the MgO{1 1 1}<sub>O</sub> substrate and became  
 256 the new terminating layer of the substrate. Similarly, for  
 257 the L-Mg/MgO{1 1 1}<sub>Mg</sub> system, during the *A/MD*  
 258 simulations the liquid Mg atoms move to the substrate  
 259 to reach thermal equilibrium (Figures 1(d) through (f)).  
 260 It is confirmed that after about 1500 steps (2.25ps),  
 261 systems reached thermal equilibrium. The resultant  
 262 equilibrium atomic configurations at terminating sur-  
 263 faces of both substrates are presented in Figure 2.  
 264 Figure 2(a) shows that some of the Mg atoms at the  
 265 MgO{1 1 1}<sub>Mg</sub> surface has moved away and became  
 266 part of the liquid, leaving a substantial amount of  
 267 vacancies (marked by the crosses) on the surface layer.  
 268 The newly formed terminating layer on the MgO{1 1  
 269 1 1}<sub>O</sub> substrate (Figure 2(b)) also contains vacancies  
 270 (marked by the crosses). A close examination of  
 271 Figures 2(a) and (b) revealed that there is no notable dif-  
 272 ference in atomic configurations at the terminating  
 273 substrate surfaces with two different starting structures  
 274 (Figures 2(a) and (b)). This suggests that the interaction  
 275 between the MgO{1 1 1} substrate and the liquid Mg  
 276 leads to the formation a new terminating surface layer  
 277 which has a hexagonal atomic arrangement of Mg  
 278 atoms and contains certain amount of vacancies,  
 279 regardless atomic configuration of the starting substrate  
 280 surface. Therefore, it can be concluded that the MgO{1  
 281 1 1} substrate in contact with liquid Mg is atomically  
 282 rough due to the existence of vacancies.

#### 283 B. Effects of the Substrate Surfaces on Prenucleation

284 Figure 3 shows snapshots of the thermally equi-  
 285 librated L-Mg/MgO{1 1 1} (Figure 3(a)) and L-Mg/  
 286 MgO{0 0 1} (Figure 3(b)) interfaces at 1000 K. Figure 3  
 287 provides us with a direct impression about the atomic  
 288 ordering in the liquid Mg adjacent to the substrates. The  
 289 liquid Mg atoms in both the L-Mg/MgO{1 1 1} and the  
 290 L-MgO{0 0 1} systems display rather weak layering. In  
 291 both cases, there is only a few identifiable atomic layers  
 292 for the liquid Mg near the substrate. These Mg atoms in  
 293 such layers show significant mobility and exhibit dom-  
 294 inantly liquid-like behavior. In addition, we noticed that  
 295 there is a distinct separation between the liquid Mg  
 296 atoms and the flat MgO{0 0 1}.

297 The density profile of liquid Mg atoms perpendicular  
 298 to a substrate surface,  $\rho(z)$ , provides a quantitative  
 299 description of the atomic layering phe-  
 300 nomenon.<sup>[11,23–25,29]</sup> We analyzed the density profiles  
 301 based on the time-averaged atomic configurations of the  
 302 simulated systems for over 3 to 6ps using Eq. (1).  
 303 The results are shown in Figure 4 for the density profiles  $\rho(z)$   
 304 and in Figure 5 for the peak density profiles  $\rho_{\text{peak}}$ . The  
 305 density profiles confirmed our first impressions about  
 306 the layering phenomenon in Figure 3. Only 4 Mg layers

The L-Mg/Mg{1 1 1}<sub>O</sub> system



The L-Mg/Mg{1 1 1}<sub>Mg</sub> system

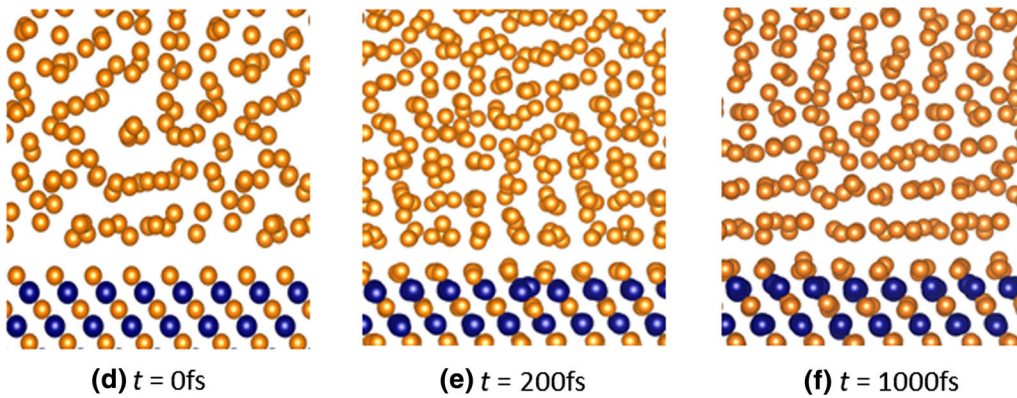


Fig. 1—Snapshots during *ab initio* molecular dynamics simulations at 1000K showing the evolution of atomic configurations in the L-Mg/MgO{1 1 1} systems from different starting configurations. (a) through (c) the L-Mg/MgO{1 1 1}<sub>O</sub> system; and (d) through (f) the L-Mg/MgO{1 1 1}<sub>Mg</sub> system. The golden spheres represent Mg atoms, and the dark blue spheres represent O atoms (Color figure online).

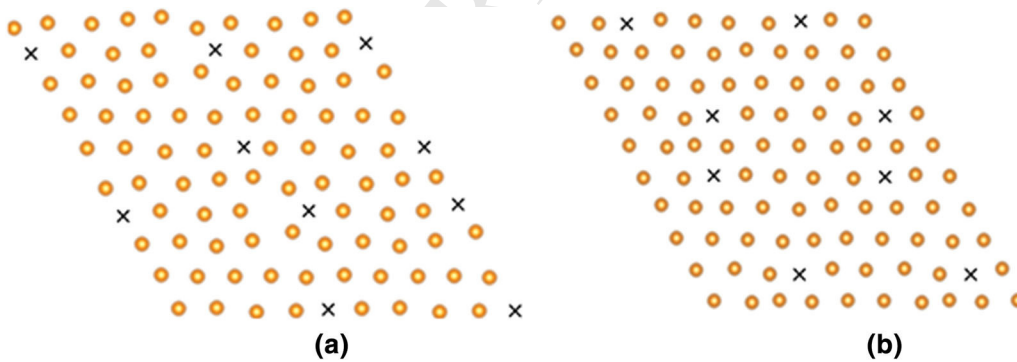


Fig. 2—Snapshots of atomic configurations (about 1ps) in the newly formed terminating Mg layer on the MgO{1 1 1} surfaces simulated at 1000K from different starting surface configurations, (a) the L-Mg/MgO{1 1 1}<sub>O</sub> system; and (b) the L-Mg/MgO{1 1 1}<sub>Mg</sub> system. The golden spheres represent Mg atoms and the crosses for vacancies (Color figure online).

307 can be recognized in the L-Mg/MgO{1 1 1} system  
 308 (Figure 4(b)) and 3 Mg layers in the L-Mg/MgO{0 0 1}  
 309 system (Figure 4(a)). In both cases, the peak heights of  
 310 liquid Mg layers are rather low as compared with those  
 311 of the substrates and decrease with increasing distance  
 312 from the interface (Figure 5).

The previous atomic molecular dynamics simulations 313  
 revealed that there are generally six layers in liquid metal 314  
 adjacent to a smooth metallic substrate.<sup>[23–25]</sup> There are 315  
 only three atomic layers of liquid Al. The lattice misfit 316  
 between MgO{1 1 1} and Mg{0 0 0 1} is 8.2 pct.<sup>[12,16]</sup> 317  
 However, as shown in the literature, lattice misfit has 318

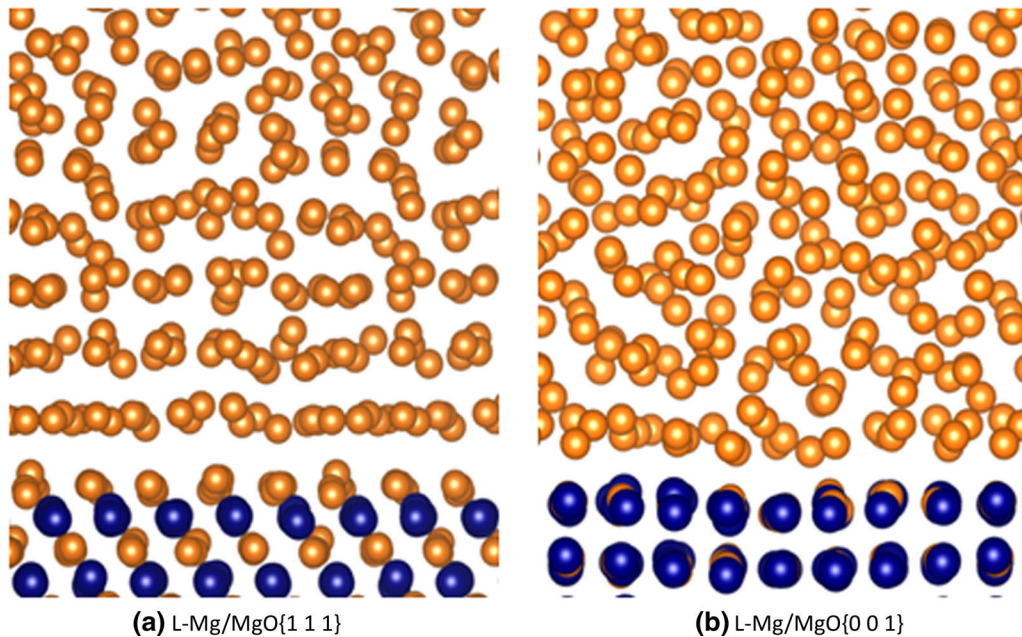


Fig. 3—Snapshots for (a) the L-Mg/MgO{1 1 1} and (b) the L-Mg/MgO{0 0 1} systems at thermodynamically equilibrated state at 1000K. The golden spheres represent Mg atoms, and the dark blue spheres represent O atoms (Color figure online).

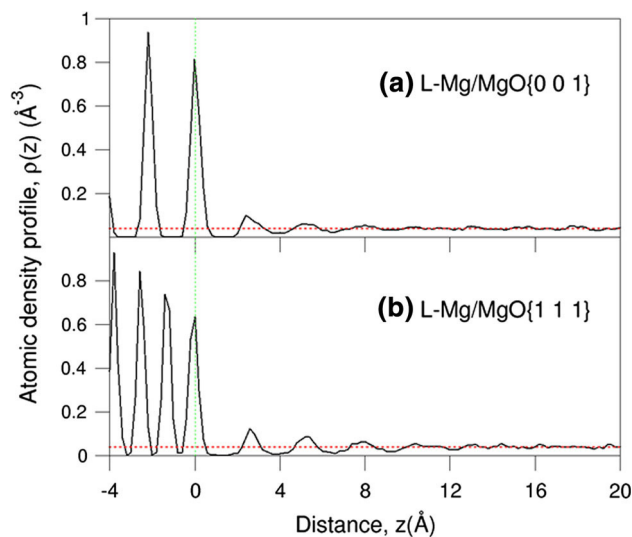


Fig. 4—Atomic density profiles,  $\rho(z)$  for (a) the L-Mg/MgO{1 1 1} system; and (b) the L-Mg/MgO{0 0 1} system at thermodynamically equilibrated state at 1000K.  $z = 0$  marks the position of terminating surface of the substrate.

319 little influence on the layering of the liquid atoms  
 320 adjacent to the substrate.<sup>[23,24]</sup> Therefore, we can con-  
 321 clude that the weakened layering in the L-Mg/MgO{1 1  
 322 1} system originates from the atomically rough substrate  
 323 surface,<sup>[26]</sup> since the atomically rough surface hinders  
 324 the templating of substrate for liquid Mg to nucleate,  
 325 according to the epitaxial nucleation/growth model.<sup>[11]</sup>

326 Figure 4 also provides information about the inter-  
 327 layer spacing between the substrate surface layer and the  
 328 1st liquid Mg layer. The interlayer spacing between the  
 329 1st Mg peak and the peak of the terminating Mg surface

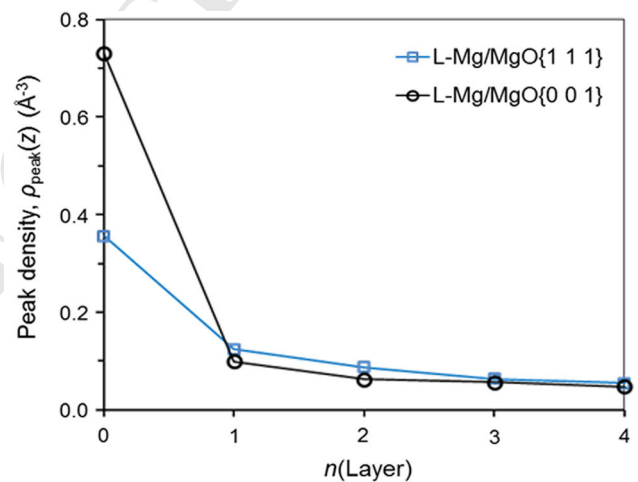


Fig. 5—Peak density,  $\rho_{\text{peak}}(z)$  for the liquid layers in the L-Mg/MgO{1 1 1} and the L-Mg/MgO{0 0 1} systems at thermodynamically equilibrated state at 1000K (Color figure online).

of the L-Mg/MgO{1 1 1} system is about 2.60 Å, which  
 331 is close to the interlayer spacing along the Mg[0 0 1]  
 332 orientation (2.61 Å). This indicates that the chemical  
 333 interaction between the MgO{1 1 1} substrate and the  
 334 liquid Mg is neutral according to our previous work.<sup>[25]</sup>  
 335 This will be discussed in the next section.

At the L-Mg/MgO{0 0 1} interface, the structurally  
 336 flat MgO{0 0 1} surface does not promote the atomic  
 337 layering in the liquid Mg. There are only three recogn-  
 338 izable Mg peaks with low peak heights (Figure 4(a)).  
 339 This is somewhat unexpected. Furthermore, a close look  
 340 at the first liquid Mg peak of the L-Mg/MgO{0 0 1}  
 341 system reveals that this Mg peak is asymmetrical.  
 342





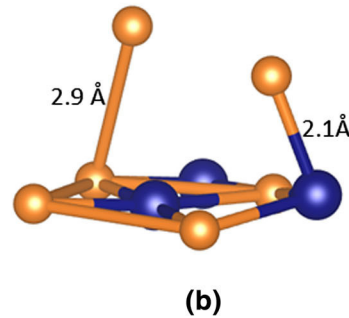
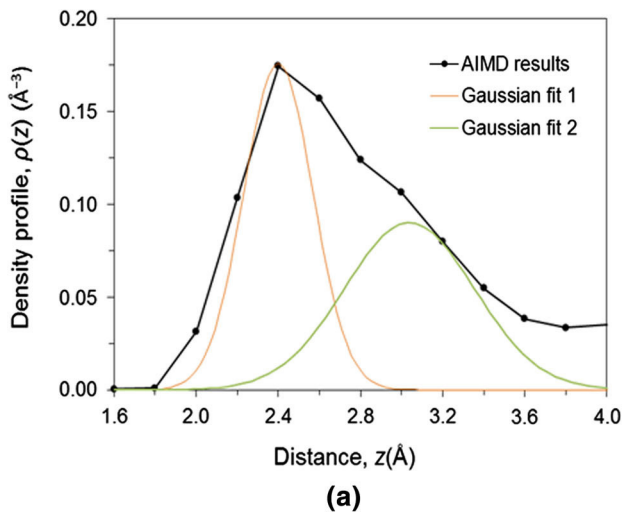


Fig. 6—(a) The density profile of the first liquid Mg layer in the L-Mg/MgO{0 0 1} system and its decomposed Gaussian peaks; and (b) The chemical bonding of liquid Mg atoms to the adjacent oxygen and magnesium ions in the MgO{0 0 1} substrate. The golden spheres represent Mg atoms, and the dark blue spheres represent O atoms. The numbers in (b) mark the bond lengths (Color figure online).

The 1st Mg peak adjacent to the MgO{0 0 1} substrate surface is enlarged and analyzed, and the results are presented in Figure 6. Apparently, this broadened and asymmetrical Mg peak contains a peak and a shoulder. Accordingly, we deconvolute it into two peaks: a peak at the position of 2.4 Å and a shoulder centered at 3.2 Å with respect to the MgO terminating layer (Figure 6(a)). Our analysis showed that the high peak at 2.4 Å is composed mainly of Mg atoms close to the O ions of the MgO{0 0 1} substrate surface, whereas the shoulder at 3.2 Å consists of Mg atoms close to the Mg ions of the substrate surface (Figure 6(b)). It is noticed that the bond length between the Mg ion at the substrate surface and the Mg atom in the liquid is 2.9 Å, being 0.8 Å longer than that between the oxygen ion and the Mg atom in the liquid (Figure 6(b)). This corresponds well to the layer spacing difference between the peak and the shoulder (0.8 Å) in Figure 6(a). This indicates that the chemistry of the MgO{0 0 1} substrate surface causes the separation of Mg atoms in the 1st liquid Mg layer. Consequently, the 1st Mg layer is atomically rough, which strongly reduces its capability to template atomic ordering in the subsequent layers.

As suggested by the epitaxial nucleation model, heterogeneous nucleation occurs *via* a layer by layer growth mechanism.<sup>[11]</sup> Therefore, the atomic ordering in an atomic layer at the liquid/substrate interface is vital to understand the nucleation potency of a substrate. Figure 7 displays the atomic arrangements of the terminating substrate layer and the first two liquid Mg layers adjacent to the substrates. Figure 8 shows the quantified in-plane order parameters of the terminating substrate layers and the liquid Mg layers from atomic configurations integrated over 3 to 6 ps, according to Eq. [2].

We first address the in-plane order parameters of the terminating layers of the substrates. As shown in Figure 7, the terminating layer of the structurally flat MgO{0 0 1} substrate shows high degree of in-plane

ordering, whereas there are vacancies in the terminating layer of MgO{1 1 1} substrate. In spite of these difference, the in-plane ordering parameter of the terminating Mg layer in L-Mg/MgO{1 1 1} system is 0.59, which is even slightly higher than that of the structurally flat MgO{0 0 1} surface  $S(z) = 0.57$  (Figure 8).

Figure 7 also shows highly delocalized characteristics of the Mg atoms even in the first Mg layer on both MgO{1 1 1} and MgO{0 0 1} substrates. This indicates that these Mg atoms exhibit mainly liquid-like behavior in the first layer. Correspondingly, the values of the in-plane order parameter,  $S(z)$  which was defined in Eq. [2] are small, being 0.01 for the 1st Mg layer on the MgO{1 1 1} substrate, and 0.08 for the first Mg layer on the MgO{0 0 1} substrate (Figure 8). Consequently,  $S(z)$  is effectively zero for the subsequently Mg layers in both cases.

To sum up, AIMD simulations showed that both atomically rough MgO{1 1 1} substrate and the structurally flat MgO{0 0 1} substrate induce only weak atomic layering and little in-plane ordering in the liquid Mg adjacent to the L-Mg/MgO interface. This suggests that those MgO substrates have poor capability to template atomic ordering in the liquid Mg and are therefore impotent for heterogeneous nucleation of solid Mg during solidification.

### C. Chemical Interaction Between Substrates and Liquid Mg

In order to obtain further insight into the atomic ordering in the liquid Mg adjacent to the substrate surface, we performed accurate electronic structure calculation and obtained electron density distributions for selected atomic configurations at the L-Mg/MgO interfaces. The iso-surfaces of electron density distributions ( $\rho_0(r) = 0.017 \text{ e}/\text{Å}^3$ ) of investigated interfaces are presented in Figure 9. As shown in Figure 9, the

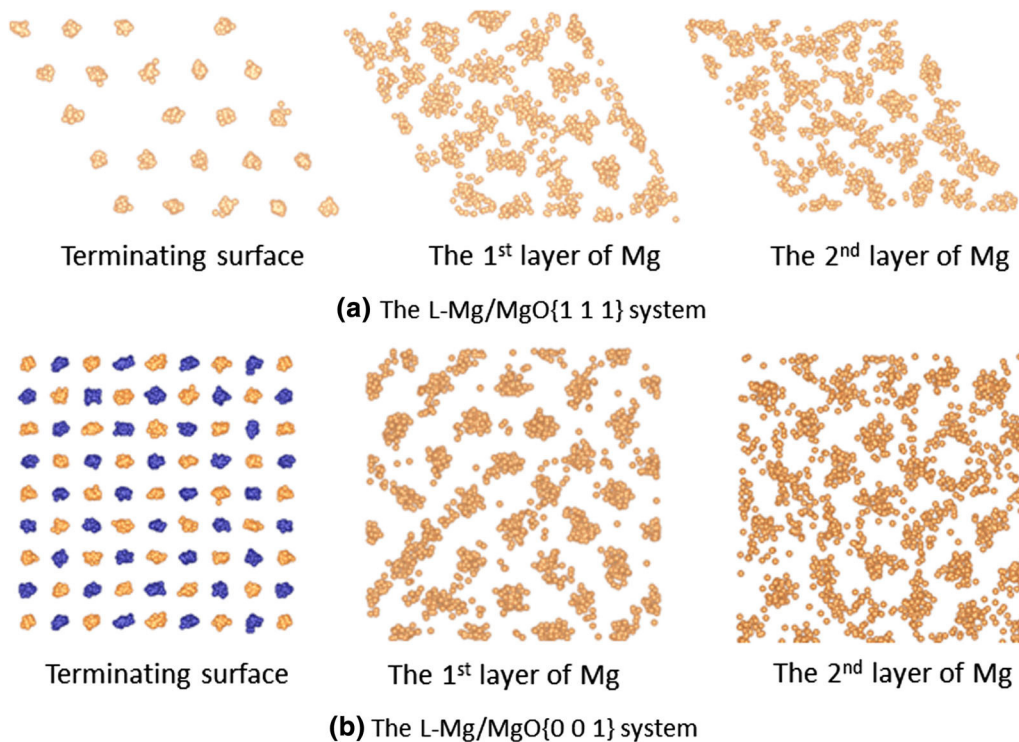


Fig. 7—Time-averaged atomic positions in the terminating surface layer and the first two liquid layers (a) for the L-Mg/MgO{1 1 1} system; and (b) for the L-Mg/MgO{0 0 1} system. The golden spheres represent Mg atoms, and the dark blue spheres represent O atoms (Color figure online).

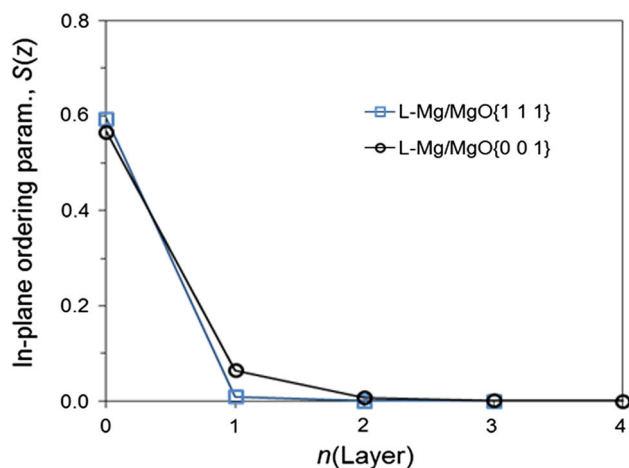


Fig. 8—In-plane order parameter,  $S(z)$  of the liquid Mg atoms as a function of the atomic layers away from the L-Mg/MgO interfaces. The  $n(\text{layer}) = 0$  represents the substrate surface (Color figure online).

419 electron density distributions of the MgO substrates  
 420 show dominantly spherical-shaped electron clouds in the  
 421 substrate regions. These spherical clouds belong to the  
 422 oxygen ions. Meanwhile, there is little electron around  
 423 the Mg ions/atoms in the MgO substrates. These results  
 424 correspond well with the ionic nature of MgO. In  
 425 addition, the liquid Mg regions are also composed of  
 426 Mg ions and electron clouds, being consistent with the  
 427 free electron nature of condensed Mg.

Charge transfer provides further information about the  
 428 interfacial chemistry.<sup>[25,38]</sup> Bader provided a unique  
 429 way to divide the boundaries of an ion/atom in a solid  
 430 via the zero flux surfaces of the electron density  
 431 distributions of a solid.<sup>[38]</sup> This model was implanted  
 432 in the code VASP.<sup>[39]</sup> Figure 10 shows the net charges at  
 433 the atomic sites for the L-Mg/MgO systems. As shown  
 434 in Figure 10, all O ions in MgO substrates have the same  
 435 net charge ( $-1.3 e$ ) and Mg ions in the substrates are  
 436 positively charged with a loss of  $1.3 e/\text{Mg}$ . This agrees  
 437 with the large electronegativity difference between Mg  
 438 ( $1.31$  in Pauling scale) and O ( $3.44$ ). Meanwhile, this  
 439 charge transfer ( $1.3 e$ ) is smaller than the pure ionic  
 440 model ( $2.0 e$ ), suggesting that although MgO is an ionic  
 441 compound, it exhibits some covalent nature.  
 442

Figure 10 shows that the terminating Mg ions at the  
 443 MgO{1 1 1} substrate surface are less charged ( $+0.6 e/\text{Mg}$   
 444 on average) as compared with those in the bulk  
 445 substrate ( $+1.3 e/\text{Mg}$ ). The Mg atoms in the first liquid  
 446 layer on the MgO{1 1 1} substrate are electronically  
 447 neutral. Therefore, the interaction between the substrate  
 448 Mg surface and liquid Mg is dominated by metallic  
 449 nature. This is consistent with the fact that the interlayer  
 450 spacing between the terminating Mg layer and the 1st  
 451 liquid Mg layer is  $2.60 \text{ \AA}$ , close to that between Mg  
 452 layers ( $2.61 \text{ \AA}$ ) (Figure 4(b)).  
 453

Interestingly, liquid Mg atoms adjacent to the struc-  
 454 turally flat MgO{0 0 1} substrate lose some electrons  
 455 (Figure 10(b)). This means that charge transfer occurs  
 456 from the liquid Mg to the substrate. This result justifies  
 457 the interpretation of the splitting of the liquid Mg  
 458

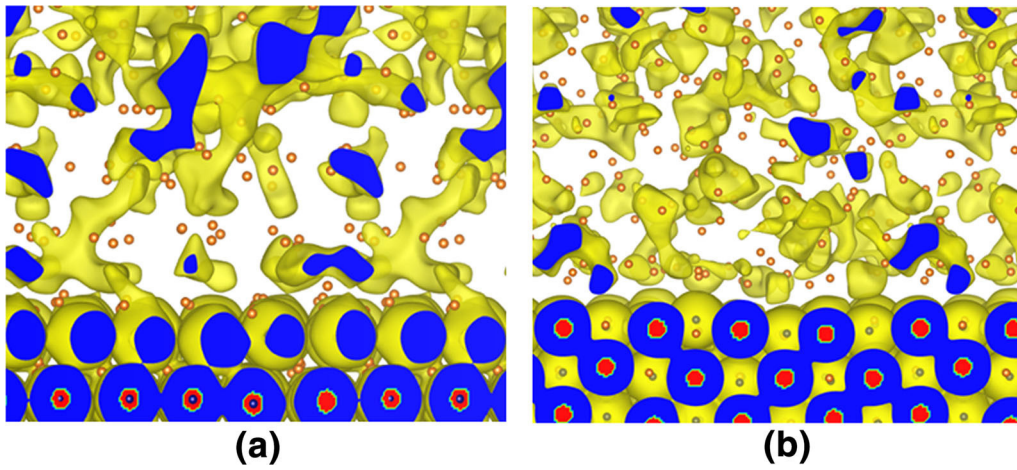


Fig. 9—The iso-surfaces of electron densities at the interfaces between liquid Mg and (a) MgO{1 1 1} substrate and (b) MgO{0 0 1} substrate. The yellow color responds to the iso-surfaces ( $\rho_0 = 0.017 \text{ e}/\text{\AA}^3$ ). The blues regions have electron density higher than  $\rho_0$ , whereas the red regions are the cross sections around cores of atoms/ions (Color figure online).

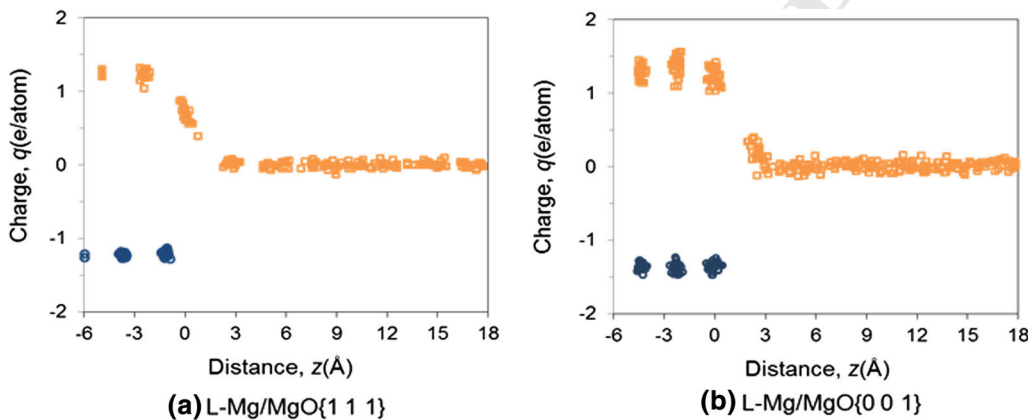


Fig. 10—The charges in the atomic/ionic spheres across the L-Mg/Mg interface with the MgO{1 1 1} substrate and the MgO{0 0 1} substrate. The distance  $z = 0$  corresponds to the center of the substrate surface. The orange squares represent the charges at Mg sites and dark blue spheres at O sites (Color figure online).

459 adjacent to the flat, non-polar MgO{0 0 1} surface.  
 460 Therefore, though MgO{0 0 1} is structurally flat,  
 461 non-polar, and stable at ambient conditions, the chem-  
 462 ical interaction between the substrate ions and the liquid  
 463 Mg atoms induces a rough Mg layer, which is similar to  
 464 effect of an atomically rough substrate surface.

#### IV. DISCUSSION

##### A. Nucleation Potency of MgO in Liquid Mg

467 In heterogeneous nucleation theory, nucleation  
 468 potency represents the intrinsic capability of a substrate  
 469 to nucleate a solid phase from the melt.<sup>[6]</sup> The nucleation  
 470 potency of a substrate can be quantified by the degree of  
 471 prenucleation that represents the capability of a sub-  
 472 strate for templating atomic ordering in the liquid  
 473 adjacent to the substrate. Prenucleation can be further  
 474 quantified by atomic layering normal to the substrate/  
 475 liquid interface and in-plane atomic ordering parallel to

the substrate/liquid interface. The recent studies of  
 prenucleation have identified the following three factors  
 that affect nucleation potency of a substrate<sup>[23–26]</sup>:

- Structural factor: The lattice misfit between a smooth substrate and a solid has a strong influence on the atomic in-plane ordering but weak on the atomic layering. A substrate surface of a smaller lattice misfit provides better structural templating for heterogeneous nucleation.<sup>[23,24]</sup>
- Chemical effect: Chemical interaction between the substrate and the liquid also influences structural templating for heterogeneous nucleation. In general, a chemically affinitive substrate promotes prenucleation, whereas a chemical repulsive substrate has lower potency for heterogeneous nucleation.<sup>[25]</sup>
- Surface roughness: The recent classic molecular dynamics simulation<sup>[26]</sup> showed that atomically rough surface impedes strongly prenucleation by reducing both atomic layering and in-plane atomic ordering in the liquid adjacent to the substrate.

496 In light of such understanding of prenucleation, we  
 497 analyze the nucleation potency of MgO in the L-Mg/  
 498 MgO system. The previous study<sup>[12,16]</sup> showed that  
 499 MgO{1 1 1} has 8.2 pct lattice misfit with solid Mg,  
 500 suggesting that MgO{1 1 1} is a poor substrate for  
 501 prenucleation. The present study has shown that  
 502 regardless the nature of starting surface termination,  
 503 MgO{1 1 1} in liquid Mg always has a Mg layer as its  
 504 new terminating surface that contain significant amount  
 505 of vacancies (Figure 2), rendering MgO{1 1 1} atomi-  
 506 cally rough. Atomic roughness of a surface can be  
 507 quantified by the arithmetical mean deviation ( $R_a$ ):

$$R_a = \left( \sum |\Delta z(i)/d_0| \right) N_z \times 100 \text{ pct} \quad [3]$$

509 where  $\Delta z(i)$  is the deviation of the  $i$ th atom from the  
 510 atomic plane along the direction perpendicular to the  
 511 substrate surface,  $d_0$  is the interlayer spacing of Mg{0 0  
 512 1}, and  $N_z$  is the total number of atoms in the layer.  
 513 When an atom is located in a crystal plane,  $\Delta z(i)/$   
 514  $d_0 = 0$ , when a lattice site is unoccupied (equivalent to  
 515 an atom is located in the next plane),  $\Delta z(i)/d_0 = 1.0$ .  
 516 Our calculation shows that there are 8.0 pct vacancies at  
 517 the terminating Mg layer of the MgO{1 1 1} substrate  
 518 (Figure 2). This corresponds to  $R_a = 8.0$  pct. There-  
 519 fore, the large lattice misfit and the large surface  
 520 roughness make the MgO{1 1 1} extremely poor for  
 521 structural templating, which in turn results in the poor  
 522 atomic layering (Figure 3) and in-plane atomic ordering  
 523 (Figure 8).

524 The formation of vacancies in the terminating Mg  
 525 layer in the L-Mg/MgO{1 1 1} system needs further  
 526 discussion. On one hand, the vacancies at the terminat-  
 527 ing Mg layer can be at least partially attributed to the  
 528 charge balance between the atoms in the terminating Mg  
 529 layer and the liquid Mg adjacent to it. Previous studies  
 530 in the literature suggested that the polar MgO{1 1 1}  
 531 surface can be stabilized at ambient conditions with only  
 532 half of the surface Mg sites being occupied.<sup>[14,15]</sup> The  
 533 present study revealed that the terminating Mg ions at  
 534 the MgO{1 1 1} substrate surface are less charged  
 535 (about + 0.6 e/Mg on average) as compared with those  
 536 in the bulk substrate (+ 1.3 e/Mg) (Figure 10). On the  
 537 other hand, the misfit between the MgO{1 1 1} and  
 538  $\alpha$ -Mg is large (8.2 pct). Therefore, the formation of  
 539 vacancies in the terminating Mg layer can be treated as a  
 540 mechanism to accommodate lattice misfit. In this sense,  
 541 the 8.2 pct lattice misfit and the 8 pct vacancies in the  
 542 L-Mg/MgO system may not cause any surprise. How-  
 543 ever, the relative contributions from accommodation of  
 544 lattice misfit (structural effect) and charge transfer  
 545 (chemical effect) warrants further investigations.

546 In addition, the L-Mg/MgO{0 0 1} system represents  
 547 another interesting case for heterogeneous nucleation.  
 548 Structurally, the MgO{0 0 1} substrate also has a large  
 549 lattice misfit with  $\alpha$ -Mg,<sup>[12,16]</sup> hindering it for heteroge-  
 550 neous nucleation. Chemically, MgO{0 0 1} surface is  
 551 non-polar under ambient conditions. However, the  
 552 situation is rather different when MgO{0 0 1} substrate  
 553 is in contact with liquid Mg. The present study has  
 554 revealed that the chemical interaction between the

MgO{0 0 1} substrate and the liquid Mg results in the  
 555 formation of a rough 1st layer of Mg atoms in the liquid  
 556 (Figure 6), which significantly reduces the potency for  
 557 structural templating of further liquid layers (Figures 4,  
 558 5, 7 and 8). As a structurally flat substrate, one would  
 559 expect pronounced layering since atomic layer is inde-  
 560 pendent of lattice misfits.<sup>[23,24]</sup> Chemistry analysis  
 561 showed the chemical interaction exists between the  
 562 substrate surface and liquid Mg. The liquid Mg atoms  
 563 adjacent to the oxygen ions are positioned closer to the  
 564 substrate due to the attractive interaction between  
 565 oxygen ions in the substrate surface and the Mg atoms  
 566 in the liquid Mg; whereas liquid Mg atoms adjacent to  
 567 the Mg ions are positioned further away from the  
 568 substrate surface because of the repulsive interaction  
 569 between the Mg ions (Figure 6). Consequently, the 1st  
 570 layer of liquid Mg atoms becomes rough and less  
 571 effective for templating atomic ordering in the further  
 572 layers. Therefore, it can be concluded that the struc-  
 573 turally flat MgO{0 0 1} substrate is also impotent for  
 574 nucleation of solid Mg.  
 575

## B. Implications to Grain Refinement of Mg-Alloys

576 The *ab initio* molecular dynamics simulations demon-  
 577 strated that both MgO{1 1 1} and MgO{0 0 1} substrate  
 578 surfaces are atomically or chemically rough and impor-  
 579 tant for heterogeneous nucleation. However, they may  
 580 be used for effective grain refinement when no other  
 581 more potent particles exist in the liquid. In spite of the  
 582 fact that heterogeneous nucleation as an atomic level  
 583 activity may occur on all available nucleant particles at a  
 584 given nucleation undercooling,<sup>[12]</sup> not all the nucleus can  
 585 lead to formation of grains in the solidified microstruc-  
 586 ture. This means that effectiveness of grain refinement  
 587 depends on the interplay between heterogeneous nucle-  
 588 ation governed by the epitaxial nucleation undercool-  
 589 ing<sup>[11]</sup> and grain initiation governed by the free growth  
 590 criterion.<sup>[40]</sup> When nucleation undercooling is smaller  
 591 than the free growth undercooling, grain initiation will  
 592 be progressive, starting with the largest particle(s) and  
 593 followed by the progressively smaller ones. Meanwhile,  
 594 when nucleation undercooling is larger than the free  
 595 growth undercooling required by many nucleant parti-  
 596 cles, a large number of nucleant particles can initiate  
 597 grains at the same time immediately after nucleation,  
 598 resulting in potentially much more significant grain  
 599 refinement. The former is called progressive grain  
 600 initiation, and the later explosive grain initiation.<sup>[12]</sup>

601 Recent research work<sup>[12,16]</sup> suggests that MgO{1 1 1}  
 602 and MgO{0 0 1} exist in Mg-alloy melt with a small  
 603 particle size, narrow size distribution, and an extremely  
 604 large number density ( $10^{17} \text{ m}^{-3}$ ). HRTEM  
 605 work<sup>[12,16,18,19]</sup> has confirmed that both MgO{1 1 1}  
 606 and MgO{0 0 1} can act as sites for heterogeneous  
 607 nucleation of  $\alpha$ -Mg. More importantly, it is confirmed  
 608 that appropriately dispersed native MgO particles can  
 609 lead to micron level grain size by high pressure die  
 610 casting of commercial purity Mg,<sup>[12]</sup> confirming that  
 611 MgO can be very effective for grain refinement of  
 612 Mg-alloys under appropriate conditions. This means  
 613 that once fully dispersed the native MgO particles can  
 614

effectively grain refine Mg-alloys without the need for any grain refiner addition. The impotency of both  $\text{MgO}\{1\ 1\ 1\}$  and  $\text{MgO}\{0\ 0\ 1\}$  particles in Mg-alloy melt from this study sheds new lights on heterogeneous nucleation, grain initiation, and grain refinement of Mg-alloys.

## V. CONCLUSIONS

Using a parameter-free *ab initio* molecular dynamics simulation technique, we investigated the atomic configurations and chemistry of  $\text{MgO}\{0\ 0\ 1\}$  and  $\text{MgO}\{1\ 1\ 1\}$  surfaces in liquid Mg. We showed that an atomically rough terminating Mg layer forms on the  $\text{MgO}\{1\ 1\ 1\}$  substrate in liquid Mg. The simulations also revealed that on the structurally flat  $\text{MgO}\{0\ 0\ 1\}$  substrate induces a rough Mg layer due to chemical interactions between the ions at the substrate surface and liquid Mg, being similar to the atomically rough  $\text{MgO}\{1\ 1\ 1\}$  substrate. The surface roughness together with the large lattice misfit with solid Mg makes both  $\text{MgO}\{1\ 1\ 1\}$  and  $\text{MgO}\{0\ 0\ 1\}$  substrate ineffective for inducing atomic ordering in the liquid adjacent to the liquid/substrate interface. It is therefore concluded that both  $\text{MgO}\{1\ 1\ 1\}$  and  $\text{MgO}\{0\ 0\ 1\}$  are impotent for heterogeneous nucleation of  $\alpha$ -Mg. The present results shed new light on grain refinement of Mg-alloys. The native MgO particles are widely available in Mg-alloy melts and may be used for effective grain refinement of Mg-alloys through explosive grain initiation without the need of grain refiner addition.

## ACKNOWLEDGMENTS

We thank Dr. H. Men (BCAST, Brunel University London) for the beneficent discussions. Financial support from EPSRC (UK) under grant number EP/N007638/1 is gratefully acknowledged.

## OPEN ACCESS

This article is distributed under the terms of the Creative Commons Attribution 4.0 International License (<http://creativecommons.org/licenses/by/4.0/>), which permits unrestricted use, distribution, and reproduction in any medium, provided you give appropriate credit to the original author(s) and the source, provide a link to the Creative Commons license, and indicate if changes were made.

## REFERENCES

1. A.L. Greer: *J. Chem. Phys.*, 2016, vol. 145, p. 211704.
2. M.A. Easton: *Solid State Mater. Sci.*, 2016, vol. 20, pp. 13–24.

3. M. Esmaily, J.E. Svensson, S. Fajardo, N. Birbilis, G.S. Frankel, S. Virtanen, R. Arrabal, S. Thomas, and G. Johansson: *Progress Mater. Sci.*, 2017, vol. 89, pp. 92–110.
4. Y.H. Ali, D. Qiu, B. Jiang, F.S. Pan, and M.Z. Zhang: *J. Alloys Compounds*, 2015, vol. 619, pp. 639–51.
5. D.H. StJohn, M. Qian, M.A. Easton, P. Cao, and Z. Hildebrand: *Metall. Mater. Trans. A*, 2005, vol. 36A, pp. 1669–79.
6. M. Qian, D.H. StJohn, and M.T. Frost: *Scripta Mater.*, 2002, vol. 46, pp. 649–54.
7. A. Ramirez, M. Qian, B. Davis, T. Wilks, and D.H. StJohn: *Scripta Mater.*, 2008, vol. 59, pp. 19–22.
8. M. Sun, M.A. Easton, D.H. StJohn, G.H. Wu, T.B. Abbott, and W.J. Ding: *Adv. Eng. Mater.*, 2013, vol. 15, pp. 373–78.
9. B. Nagasivamuni, G. Wang, D.H. StJohn, and M.S. Dargusch: *J. Crystal Growth*, 2019, vol. 512, pp. 20–32.
10. W.C. Yang, L. Lin, J. Zhang, S.X. Ji, and Z. Fan: *Mater. Lett.*, 2015, vol. 160, pp. 263–67.
11. Z. Fan: *Metall. Mater. Trans. A*, 2013, vol. 44A, pp. 1409–18.
12. Z. Fan, F. Gao and B. Jiang: submitted to *science*, 2018.
13. H. Men, B. Jiang, and Z. Fan: *Acta Mater.*, 2010, vol. 58, pp. 6526–34.
14. P.W. Tasker: *Philos. Mag. A*, 1979, vol. 39, pp. 119–36.
15. C.M. Fang, M.A. Van Huis, D. Vanmaekelbergh, and H.W. Zandbergen: *ACS Nano*, 2010, vol. 4, pp. 211–18.
16. G.S. Peng, Y. Wang, and Z. Fan: *Metall. Mater. Trans. A*, 2018, vol. 49A, pp. 2182–92.
17. Z. Fan, Y. Wang, M. Xia, and S. Arumuganathar: *Acta Mater.*, 2009, vol. 57, pp. 4891–4901.
18. Y. Wang, Z. Fan, X. Zhou, and G.E. Thompson: *Philos. Mag. Lett.*, 2011, vol. 91, pp. 516–29.
19. Y. Wang, G.S. Peng and Z. Fan: *Magnesium Technology 2017*, eds. K.S. Solanki, et al. The Minerals, Metals & Materials Series, 2017, pp. 99–106.
20. E.T. Dong, P. Shen, L.X. Shi, D. Zhang, and Q.C. Jiang: *J. Mater. Sci.*, 2013, vol. 48, pp. 6008–17.
21. W.W. Xu, A.P. Horsfield, D. Wearing, and P.D. Lee: *J. Alloys Compounds*, 2016, vol. 68, pp. 1233–40.
22. H.-Q. Song, M. Zhao, and J.G. Li: *Modern Phys. Lett. B*, 2016, vol. 30, p. 165052.
23. H. Men and Z. Fan: *Comp. Mater. Sci.*, 2014, vol. 85, pp. 1–7.
24. H. Men and Z. Fan: *Metall. Mater. Trans. A*, 2018, vol. 49A, pp. 2766–77.
25. C.M. Fang, H. Men, and Z. Fan: *Metall. Mater. Trans. A*, 2018, vol. 49A, pp. 6231–42.
26. B. Jiang, H. Men, and Z. Fan: *Comp. Mater. Sci.*, 2018, vol. 153, pp. 73–81.
27. R.R. Reeber, K. Goessel, and K. Wang: *Eur. J. Mineral.*, 1995, vol. 7, pp. 1039–47.
28. J.W. Arblaster: *Selected values of the crystallographic properties of the elements*, ASM International, Materials Park, Ohio, 2018.
29. A. Hashibon, J. Adler, M.W. Finnis, and W.D. Kaplan: *Comput. Mater. Sci.*, 2002, vol. 24, pp. 443–52.
30. G. Kresse and J. Hafner: *Phys. Rev. B*, 1994, vol. 49, pp. 14251–69.
31. G. Kresse and J. Furthmüller: *Comput. Mater. Sci.*, 1996, vol. 6, pp. 15–50.
32. P.E. Blöchl: *Phys. Rev. B*, 1994, vol. 50, pp. 17953–79.
33. G. Kresse and J. Joubert: *Phys. Rev. B*, 1999, vol. 59, pp. 1758–75.
34. J.P. Perdew, K. Burke, and M. Ernzerhof: *Phys. Rev. Lett.*, 1996, vol. 77, pp. 3865–68.
35. H.J. Monkhorst and J.D. Pack: *Phys. Rev. B*, 1976, vol. 13, pp. 5188–92.
36. G.A. de Wijs and G. Kresse: *Phys. Rev. B*, 1998, vol. 57, pp. 8223–34.
37. C.M. Fang, R.S. Koster, W.-F. Li, and M.A. van Huis: *RSC Adv.*, 2014, vol. 4, pp. 7885–99.
38. R.F.W. Bader: *J. Phys. Chem. A*, 1998, vol. 102, pp. 7314–23.
39. W. Tang, E. Sanville, and G. Henkelman: *J. Phys.*, 2009, vol. 21, p. 084204.
40. A.L. Greer, A.M. Bunn, A. Tronche, P.V. Evans, and D.J. Bristow: *Acta Mater.*, 2000, vol. 48, pp. 2823–35.

**Publisher's Note** Springer Nature remains neutral with regard to jurisdictional claims in published maps and institutional affiliations.



Journal : **MMTA**

Dispatch : **12-11-2019**

Pages : **10**

PIPS No. : **5495**

LE

TYPESET

MS Code :

CP

DISK

Journal : **11661**

Article : **5495**

## Author Query Form

**Please ensure you fill out your response to the queries raised below and return this form along with your corrections**

Dear Author

During the process of typesetting your article, the following queries have arisen. Please check your typeset proof carefully against the queries listed below and mark the necessary changes either directly on the proof/online grid or in the 'Author's response' area provided below

Query	Details Required	Author's Response
AQ1	Kindly update complete page range for References [1, 39, 22]. And also update complete details for Ref. [12].	